CRYSTAL GROWTH & DESIGN

Article

pubs.acs.org/crystal

How Structure-Directing Cations Tune the Fluorescence of Metal–Organic Frameworks

Published as part of the Crystal Growth & Design Mikhail Antipin Memorial virtual special issue

Carlos Ordonez,[†] Marina Fonari,[†,§] Jennifer Lindline,[‡] Qiang Wei,*[,†] and Tatiana Timofeeva*[,†]

[†]Department of Biology and Chemistry and [‡]Department of Natural Resources Management, New Mexico Highlands University, Las Vegas, New Mexico 87701, United States

[§]Institute of Applied Physics Academy of Sciences of Moldova, Academy str., 5 MD2028, Chisinau, Moldova

Supporting Information

ABSTRACT: A series of metal-organic frameworks (MOFs), {Zn-BTC}{cations}, which contain anionic Zn-BTC coordination polymers, is reported here. It was observed that cations with different hydrogen-bond forming abilities could significantly affect the coordination of Zn-BTC structures in the frameworks. The 13 Zn-BTC MOFs reported herein showed solid-state fluorescent emission in the visible spectrum, and the fluorescence of the frameworks was tunable by adjusting the interactions of the cations with the anionic Zn-BTC structure in the MOFs.

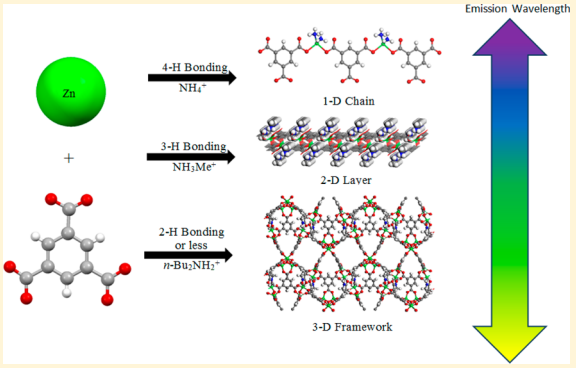

INTRODUCTION

Synthesizing and controlling the functionality of highly structurally engineered materials are always a fascinating target in both the industrial side of applications and the academic side of research.[1] Metal–organic frameworks (MOFs) are among such structurally engineered materials that possess a wide array of potential and realized applications, including drug delivery, gas storage, light emitting materials, chemical separation, and as light emitting and semiconductor materials.[2] During the past two decades, scientists have not only synthesized thousands of MOFs with highly accessible porous structures but also learned how to predict and control the topology of the frameworks[3] and their resultant functionality.[4−6] MOFs with luminescent functionality have attracted much effort in materials chemistry aimed toward applications in light-emitting and display devices, sensors for environmental or physical stimulations, and biomedical engineering.[5] MOFs with tunable fluorescence[7] have attracted great interest in the research field due to their multiple applications and facile tenability. We report a study of a series of anionic MOFs with tunable fluorescence controlled by the included countercations. MOFs with anionic frameworks were constructed from Zn^{2+} with 1,3,5-benzenetricarboxylate (BTC) organic anions. We examined the influence of various countercations such as NH^{4+}, $MeNH^{3+}$, Me_2NH^{2+}, Et_3NH^{+}, and n-Bu_4N^{+} to observe the structural changes of the anionic Zn-BTC connectivity within the frameworks and the fluorescence of the corresponding MOFs. For instance, utilization of the NH^{4+} cation resulted in a one-dimensional chain structure of Zn-BTC, while the $MeNH^{3+}$ cation can result in a two-dimensional layer of Zn-BTC in the crystal. Cations such as Me_2NH^{2+}, Et_3NH^{+}, and n-Bu_4N^{+}, which have two or less hydrogen bonding sites, can generate three-dimensional framework structures. Correspondingly, the MOF incorporating NH^{4+} as the countercation emitted light in the violet region of the visible spectrum, while incorporating n-Bu_4N^{+} as the countercation shifted the resulting emitted light wavelength to the blue region. Furthermore, frameworks with 1-butyl-3-methylimidazolium (BMIM) cations can emit light in the green region. Our study developed an understanding of the MOFs' structure–property relationship in fluorescent tenability, where the key criteria are the differences in interactions (electrostatic and/or hydrogen bonding) between the cations with an anionic Zn-BTC backbone in their framework. All compounds utilized in this study are shown in Scheme 1.

EXPERIMENTAL SECTION

Materials and Measurements. All of the solvents and reagents for synthesis were commercially available and used as received. Powder X-ray diffraction (PXRD) spectra were recorded on a GBC Mini Materials Analyzer powder X-ray diffractometer operating at 35 kV and 30 mA using Cu Kα radiation (λ = 1.5418 Å). The 2θ angles were recorded from 5° to 40°. Solid-state fluorescence spectra were performed on a Shimadzu RF-5301 PC spectrofluorophotometer with a xenon lamp light source at ambient temperature.

Received: April 29, 2014
Revised: September 4, 2014
Published: September 9, 2014

   dx.doi.org/10.1021/cg5006133 | Cryst. Growth Des. 2014, 14, 5452–5465

Scheme 1. Organic Ligands, Solvents, and Cations Applied in This Research

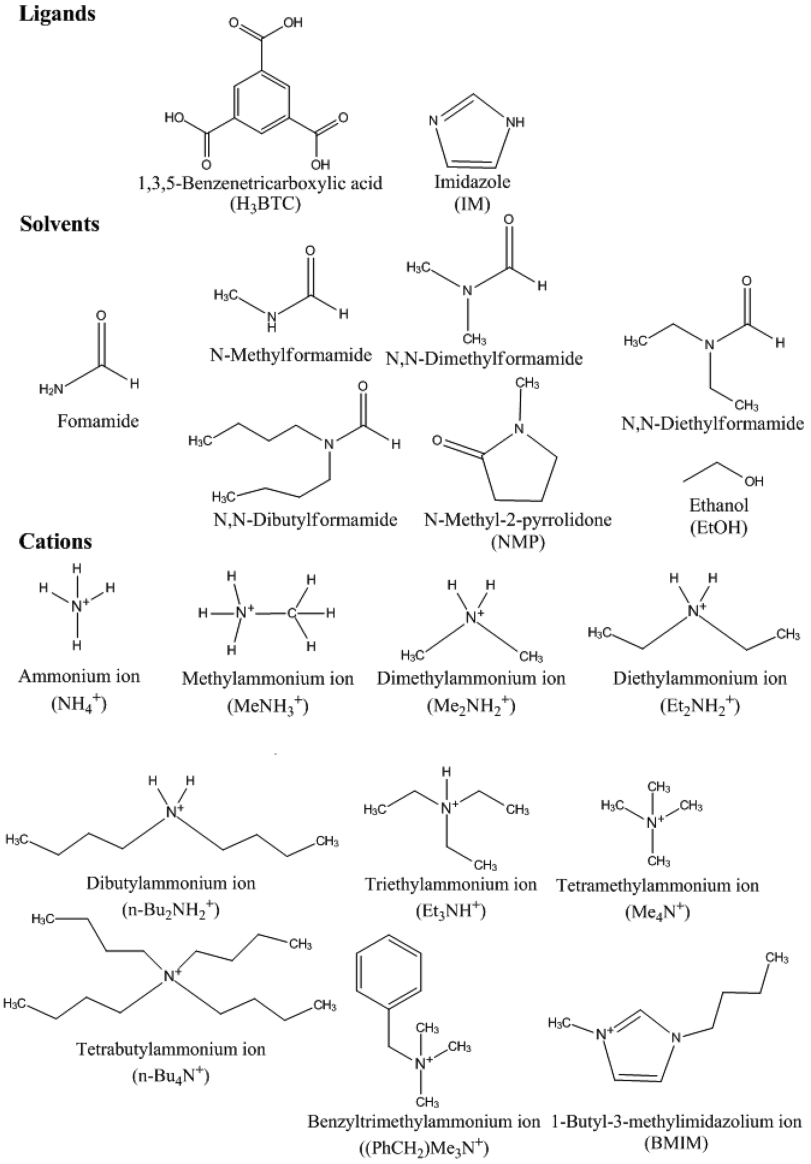

Table 1. Summary of Reaction Conditions for Method 1

cation	$Zn(NO_3)_2{\cdot}6H_2O$ (g, mmol)	H_3BTC (g, mmol)	formamide 1 (mL)	solvent 2 (mL)	yield (%)
NH_4^+	0.3, 1.0	0.21, 1.0	formamide 5	ethanol, 5	25
$MeNH_3^+$	1.5, 5.1	1.05, 5.0	*N*-methylformamide, 25	ethanol, 25	39
$Me_2NH_2^+$	1.5, 5.1	1.05, 5.0	*N*,*N*-dimethylformamide, 50		77
$Et_2NH_2^+$	0.3, 1.0	0.21, 1.0	*N*,*N*-diethylformamide, 5	ethanol, 5	57
n-$Bu_2NH_2^+$	0.15, 0.5	0.105, 0.5	*N*,*N*-dibutylformamide, 5	ethanol, 5	33

Table 2. Summary of Reaction Conditions for Method 2

cation	$Zn(NO_3)_2{\cdot}6H_2O$ (g, mmol)	H_3BTC (g, mmol)	base (g, mmol)	solvent (mL)	yield (%)
n-$Bu_2NH_2^+$	0.343, 1.15	0.244, 1.16	dibutylamine 0.142, 1.10	NMP, 10	11
Et_3NH^+	1.5, 5.1	1.05, 5.0	triethylammine 25 mL	ethanol, 25	35
imidazole	0.15, 0.51	0.105, 0.5	imidazole 0.034, 0.5	NMP, 15	10
imidazole	0.75, 2.5	0.525, 2.5	imidazole 0.34, 5	NMP, 50	26

Synthesis. *Method 1: Decomposition of Formamides.* A mixture of $Zn(NO_3)_2{\cdot}6H_2O$ (1.5 g, 5.1 mmol), 1,3,5-benzenetricarboxylic acid, H_3BTC (1.05 g, 5.0 mmol), and dimethylformamide (50 mL) was dissolved in a beaker. The solution was transferred to a 125 mL Teflon-lined acid digestion vessel. The vessel was placed in an oven set at 150 °C for 3 days. After 3 days the oven was turned off, and the acid digestion vessel was allowed to cool slowly overnight. The crystals were collected, washed with fresh dimethylformamide, and sonicated for 2 min to remove any remaining unreacted starting materials. Washing and sonication were performed twice to ensure the purity of

dx.doi.org/10.1021/cg5006133 | *Cryst. Growth Des.* 2014, 14, 5452−5465

Table 3. Summary of Reaction Conditions for Method 3

cation	$Zn(NO_3)_2{\cdot}6H_2O$ (g, mmol)	H_3BTC (g, mmol)	salt (g, mmol)	solvent 1 (mL)	solvent 2 (mL)	yield (%)
Me_4N^+	0.361, 1.2	0.255, 1.2	tetramethyl-ammonium hydroxide pentahydrate 0.37, 2.0	NMP 50		5
n-Bu_4N^+	3.61, 12.1	2.55, 12.1	tetrabutyl- ammonium nitrate 3.7, 12.2	NMP 50		21
$(PhCH_2)Me_3N^+$	1.5, 5.1	1.05, 5.0	benzyltrimethyl-ammonium chloride 0.938, 5.1	ethanol 50		11
BMIM (ionic liquid)	0.3, 1.0	0.21, 1.0		NMP 5	1-butyl-3-methyl-imidazolium tetrafluoro-borate 5	11

the sample. The resulting crystals were plate shaped and clear (% yield = 77%). The conditions of synthesis of the MOFs by method 1 are listed in Table 1.

Method 2: Addition of Base. A mixture of $Zn(NO_3)_2{\cdot}6H_2O$ (0.343 g, 1.15 mmol), H_3BTC (0.244g, 1.16 mmol), dibutylamine base (0.142 g, 1.10 mmol), and *N*-methylpyrrolidone (NMP, 10 mL) was prepared in a capped vial. The solution was transferred to a 23 mL Teflon-lined acid digestion vessel and placed in the oven at 150 °C for 4 days. The produced crystals were collected in a vial, washed with fresh NMP, and sonicated to remove impurities from the crystals. The resulting crystals were plate shaped and yellow (% yield = 11%). The conditions of synthesis of the MOFs by method 2 are listed in Table 2.

Method 3: Direct Addition of Cations. A mixture of $Zn(NO_3)_2{\cdot}6H_2O$ (3.61 g, 12.1 mmol), H_3BTC (2.55 g, 12.1 mmol), tetrabutylammonium nitrate (3.70 g, 12.2 mmol), and NMP (50 mL) was dissolved in a beaker. The solution was sonicated, placed in a 125 mL Teflon-lined acid digestion vessel, and heated for 3 days at 150 °C. The resulting crystals were large, plate-shaped, yellow crystals (% yield = 21%). The amount of compounds used for the synthesis of each MOF, the solvents used, and the yields obtained are outlined in Table 3.

X-ray Crystallography. Single crystals of each compound were selected using a cross-polarized light microscope. Each crystal data set was collected by a Bruker APEX-II CCD diffractometer using the SAINT+ v. 6.2 software[8] with graphite-monochromated Mo–Kα radiation using phi/omega scans. The crystal was mounted onto the diffractometer at a temperature of 100 K under liquid nitrogen. Three scans were performed with 364 frames for each scan. The structures were solved and refined utilizing the SHELXTL program package,[9] and the non-hydrogen atoms were refined with anisotropic thermal parameters. Hydrogen atoms were added at idealized positions, and a riding model was used for subsequent refinement. The function minimized was $\Sigma[w(|F_o|^2 - |F_c|^2)]$ with reflection weights $w - 1 = [\sigma^2|F_o|^2 + (g_1P)^2 + (g_2P)]$ where $P = [\max |F_o|^2 + 2|F_c|^2]/3$. Crystallographic data for all of the compounds reported in the study are displayed in Table 4.

RESULTS AND DISCUSSION

Introduction of Cations in the Synthesis. Anionic MOFs with cations residing in the voids of the frameworks are relatively rare as compared to neutral or cationic MOFs.[10] The reaction of divalent metal ions, such as Zn^{2+}, with trivalent anoins, such as 1,3,5-benzenetricarboxylate (BTC), may be one of the easiest ways to form anionic frameworks where countercations reside in the void spaces. In this study, $Zn(NO_3)_2{\cdot}6H_2O$ salt and the neutral H_3BTC ligand were dissolved in organic solvents, and the system was heated with corresponding cations under solvothermal conditions to form crystals. Three methods were utilized to introduce the cations needed in the frameworks. Method 1 was in situ generation of cations from the decomposition of formamides. For example, NH_4^+, $MeNH_3^+$, and $Me_2NH_2^+$ were generated from formamide, *N*-methylformamide and *N*,*N*-dimethylformamide, respectively. The second method utilized amine bases to generate corresponding organic ammonium cations, such as in the case of Et_3NH^+ and n-$Bu_2NH_2^+$ cations. The third method was directly adding cations, such as quaternary ammonium n-Bu_4N^+ and Me_4N^+ in the reaction. The synthetic conditions for introducing different cations are summarized in Tables 1, 2, and 3.

When applying the first method to introduce the cations, the corresponding formamides could be utilized directly as solvents. However, when using the second or third methods to introduce the cations, NMP or a mixture of NMP with EtOH were used as the solvents. In some cases, EtOH was mixed with the formamides in method 1 in order to generate better quality crystals. Imidazole (IM) was planned to be introduced as a base to the reaction system with the aim to generate the imidazolium cations; however, the results revealed a neutral framework with imidazole acting as a coordinating ligand to the Zn(II) in the frameworks. In this study, the reaction system was typically heated at 150 °C for 3 days and allowed to cool to room temperature naturally in the oven. A longer reaction time in method 3 was required to achieve better crystalline samples for single-crystal X-ray crystallography analysis.

Influence of Cations on the Crystal Structural Changes. With the exception of imidazole, the MOFs formed in this study all contained anionic Zn-BTC coordination polymers with cations in their structures. It was observed that the dimensionality of the anionic Zn-BTC coordination polymer was strongly related with the hydrogen-bond forming ability of the used cations. It was found that if the cations have four H-bonding sites, the anionic Zn-BTC formed a one-dimensional chain structure; if the cations can form three H-bondings, Zn-BTC formed a 2D layer structure; and when the cations have two or less H-bonding sites, the 3D frameworks of Zn-BTC formed. One possible explanation for the differences in the crystallographic structure that developed may be that at the first stage of the deprotonation of H_3BTC ligands in the reaction, the cations form complexes with the BTC anions by H-bondings. When cations have more H-bonding forming sites, fewer accessible carboxylate groups of BTC are involved in the coordination with Zn(II) ions. Therefore, the higher H-bonding results in lower dimensional structures. The crystallographic characteristics of MOFs are summarized in Table 4 and described in the following context.

One-Dimensional Chain Anionic Structure for Cation with Four H-bonding Capability. In the case of MOF {Zn-BTC}{NH_4^+}, BTC ligands are connected through only two carboxylate groups with single zinc ions to form 1D chain structures, as shown in Figure 1. Each Zn(II) is tetrahedrally coordinated by two carboxylate groups from BTC in a monodentate binding mode and two NH_3 molecules. Those chains are packed to form layers, and NH_4^+ cations are located between the layers in the structure.

Two-Dimensional Layer Anionic Structure for Cation with Three H-bonding Capability. Unlike MOF {Zn-

dx.doi.org/10.1021/cg5006133 | Cryst. Growth Des. 2014, 14, 5452–5465

Table 4. Crystallographic Data and Structure Refinement Details for MOF {Zn-BTC}{cations}

MOFs	{Zn-BTC}{NH_4^+}	{Zn-BTC}{$MeNH_3^+$}	{Zn-BTC}{$Me_2NH_2^+$}	{Zn-BTC}{$Et_2NH_2^+$}	{Zn-BTC}{n-$Bu_2NH_2^+$}-M1	{Zn-BTC}{n-$Bu_2NH_2^+$}-M2
formula	$C_{10}H_{16}N_4O_7Zn$	$C_{10}H_9NO_6Zn$	$C_{14}H_{18}N_2O_7Zn$	$C_{14.25}H_{17.75}N_{1.25}O_{6.25}Zn$	$C_{17}H_{23}NO_6Zn$	$C_{28.50}H_{71}N_5O_{35}Zn_8$
formula weight	369.64	304.55	391.67	371.92	402.73	1566.86
crystal system	triclinic	triclinic	monoclinic	monoclinic	monoclinic	monoclinic
space group	$P\bar{1}$	$P\bar{1}$	$P2_1/n$	$P2_1/n$	$P2_1/c$	$C2/c$
a (Å)	8.333(3)	7.791(3)	9.4299(13)	9.509(3)	9.488(6)	10.284(5)
b (Å)	9.780(4)	8.989(4)	16.490(2)	15.180(4)	12.562(9)	35.000(18)
c (Å)	10.670(4)	9.160(4)	11.280(15)	12.246(3)	15.477(10)	25.542(13)
α (deg)	67.335(5)	116.446(5)	90	90	90	90
β (deg)	68.389(5)	104.488(5)	97.731(2)	93.835(4)	106.099(10)	97.980(9)
γ (deg)	68.702(5)	98.089(5)	90	90	90	90
V (Å^3)	720.8(5)	532.0(4)	1738.2(4)	1763.7(8)	1772(2)	9105(8)
Z	2	2	4	4	4	4
D_{calc} (Mg/m^3)	1.703	1.901	1.497	1.401	1.509	1.143
μ(Mo Kα) (mm^{-1})	1.746	2.329	1.450	1.420	1.418	2.130
F(000)	380	308	808	768	840	3188
total reflections	6258	5340	17032	20833	11541	31105
unique reflections	2956	2559	4180	5433	2539	6540
R(int)	0.0193	0.0225	0.0328	0.0416	0.0878	0.0806
R_1 [$I > 2\sigma(I)$]	0.0244	0.0288	0.0279	0.0407	0.0494	0.0661
wR_2 [$I > 2\sigma(I)$]	0.0564	0.0699	0.0660	0.1011	0.1119	0.1871
R_1 (all data)	0.0289	0.0344	0.0370	0.0573	0.0762	0.0877
wR_2 (all data)	0.0585	0.0729	0.0698	0.1098	0.1265	0.2073
GOF on F^2	1.052	1.046	1.046	1.048	1.037	1.020

compound	{Zn-BTC}{Et_3NH^+}	{Zn-BTC}{Me_4N^+}	{Zn-BTC}{n-Bu_4N^+}	{Zn-BTC}{$(PhCH_2)Me_3N^+$}	{Zn-BTC}{BMIM}
formula	$C_{15}H_{19}NO_6Zn$	$C_{96}H_{134}N_{10}O_{39}Zn_5$	$C_{48}H_{41}N_2O_{20}Zn_4$	$C_{38}H_{38}N_2O_{12}\ Zn_2$	$C_{17}H_{18}N_2O_6Zn$
formula weight	374.68	2378.98	1227.31	845.44	411.70
crystal system	monoclinic	monoclinic	monoclinic	orthorhombic	monoclinic
space group	$P2_1/n$	$P2_1/n$	$C2/c$	$Pna2_1$	$P2_1/n$
a (Å)	9.460(16)	23.31(2)	33.843(12)	32.407(6)	9.2987(14)
b (Å)	15.98(3)	18.952(18)	9.954(3)	9.5750(18)	16.670(2)
c (Å)	11.574(20)	26.57(2)	35.817(12)	12.193(2)	11.4189(17)
β (deg)	93.89(2)	94.757(14)	106.562(5)	90	108.481(3)
V (Å^3)	1745(5)	11696(19)	11566(7)	3783.3(12)	1678.7(4)
Z	4	4	8	4	4
D_{calc} (g cm^{-3})	1.426	1.351	1.410	1.484	1.629
μ(Mo Kα) (mm^{-1})	1.434	1.093	1.709	1.333	1.501
F(000)	776	4968	4984	1744	848
total reflections	8858	44967	35221	17492	9968
unique reflections	1864	9056	7730	3930	2849
R(int)	0.2107	0.1826	0.1014	0.1129	0.0681
R_1 [$I > 2\sigma(I)$]	0.0761	0.0795	0.1172	0.0476	0.0501
wR_2 [$I > 2\sigma(I)$]	0.1737	0.1848	0.2540	0.0963	0.1146
R_1 (all data)	0.1314	0.1391	0.1481	0.0736	0.0819

dx.doi.org/10.1021/cg5006133 | Cryst. Growth Des. 2014, 14, 5452−5465

Table 4. continued

compound	{Zn-BTC}{Et_3NH^+}	{Zn-BTC}{Me_4N^+}	{Zn-BTC}{n-Bu_4N^+}	{Zn-BTC}{$(PhCH_2)Me_3N^+$}	{Zn-BTC}{BMIM}
wR_2 (all data)	0.2016	0.2231	0.2697	0.1100	0.1337
GOF on F^2	1.016	1.015	1.181	1.085	1.026

compound	{Zn-BTC-IM}	{Zn-BTC-2IM}
formula	$C_{36}H_{37.5}N_5O_{15}Zn_3$	$C_{75}H_{71}N_{19}O_{27}Zn_6$
formula weight	976.32	2062.73
crystal system	monoclinic	monoclinic
space group	$P2_1/n$	$C2/m$
a (Å)	12.366(2)	26.656(15)
b (Å)	13.439(3)	24.838(14)
c (Å)	26.969(5)	10.191(6)
β (deg)	95.463(3)	110.667(7)
V (Å^3)	4461.5(15)	6313(6)
Z	4	2
D_{calc} (g cm^{-3})	1.454	1.085
μ(Mo Kα) (mm^{-1})	1.668	1.182
F(000)	1994	2100
total reflections	27980	20708
unique reflections	6328	4622
R(int)	0.0472	0.0738
R_1 [$I > 2\sigma(I)$]	0.0946	0.0993
$wR2$ [$I > 2\sigma(I)$]	0.2630	0.2622
R_1 (all data)	0.1098	0.1162
wR_2 (all data)	0.2772	0.2720
GOF on F^2	1.017	1.166

dx.doi.org/10.1021/cg5006133 | Cryst. Growth Des. 2014, 14, 5452−5465

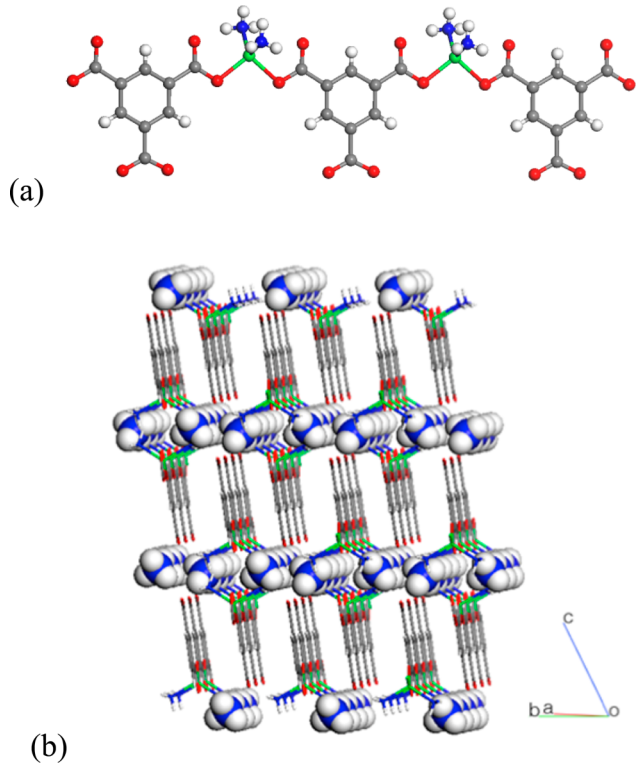

Figure 1. (a) One-dimensional structure of anionic Zn-BTC. (b) Packing diagram of chains in MOF {Zn-BTC}{NH_4^+}. Zn = green, N = blue, O = red, and C = gray. Molecules of formamide are omitted for clarity.

BTC}{NH_4^+}, MOF {Zn-BTC}{$MeNH_3^+$} contains [$Zn_2(\mu$-$OOC)_2$] dimers in the frameworks, and those dimers are connected through BTC ligands to form a double-layer anionic framework (Figure 2). Each [$Zn_2(\mu$-$OOC)_2$] is surrounded by six BTC ligands, which are parallel to each other. Each Zn(II) is still in a tetrahedral coordination with the four carboxylate groups of BTC, and each BTC ligand uses one carboxylate group to bridge two Zn atoms to form the [$Zn_2(\mu$-$OOC)_2$] dimer structure and uses the remaining two carboxylate groups to connect the surrounding Zn_2 dimers to form the double-layer structure. The methyl groups of the $MeNH_3^+$ cations are located inside the double layers, while the -NH_3 parts approach out of the layers to form hydrogen bonds with nearby layers in a closed packing structure.

Three-Dimensional Framework Anionic Structure for Cation with Two or Less H-Bonding Capability. It was found that when cations have two or fewer hydrogen-bond forming abilities, the 3D framework structures of anionic Zn-BTC formed. In this catalog, the size and shape of the cations can influence the 3D framework structures. However, among those 3D frameworks, the most common anionic Zn-BTC structure observed was in MOF {Zn-BTC}{$Me_2NH_2^+$}. In this structure, [$Zn_2(\mu$-$OOC)_2$] motifs were also formed, and each motif was surrounded by six BTC ligands. However, contrary to those in MOF {Zn-BTC}{$MeNH_3^+$}, four BTC ligands were now located in the same plane, while two of the BTC ligands were found in the near perpendicular planes. Such a connection of [$Zn_2(\mu$-$OOC)_2$] motifs results in the X-shaped chains cross-linked with each other to form a channeled Zn-BTC anionic framework (Figure 3).

If the [$Zn_2(\mu$-$OOC)_2$] structure motif and BTC are seen as second building units (SBUs), then the Zn-BTC framework can be seen as a (3,6)-connected net; i.e., one BTC ligand connects three Zn_2 units, and each Zn_2 unit connects six BTC ligands. The Zn-BTC anionic framework in MOF {Zn-BTC}-{$Me_2NH_2^+$} therefore has the same topology as rutile, TiO_2. The topologic similarity between TiO_2 and MOF {Zn-BTC}{$Me_2NH_2^+$} is shown in Figure 4.

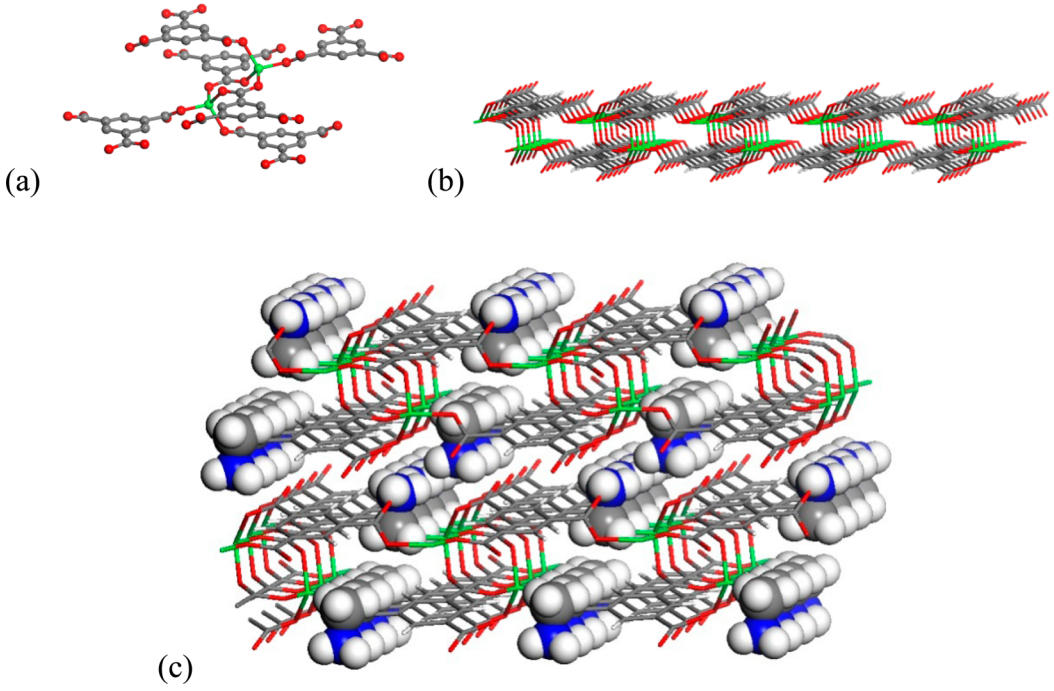

Figure 2. (a) The [$Zn_2(\mu$-$OOC)]_2$ dimer with coordinated six BTC ligands. (b) The double-layer structure of Zn-BTC. (c) The packing of the double layers viewed along the *a* axis.

dx.doi.org/10.1021/cg5006133 | *Cryst. Growth Des.* 2014, 14, 5452−5465

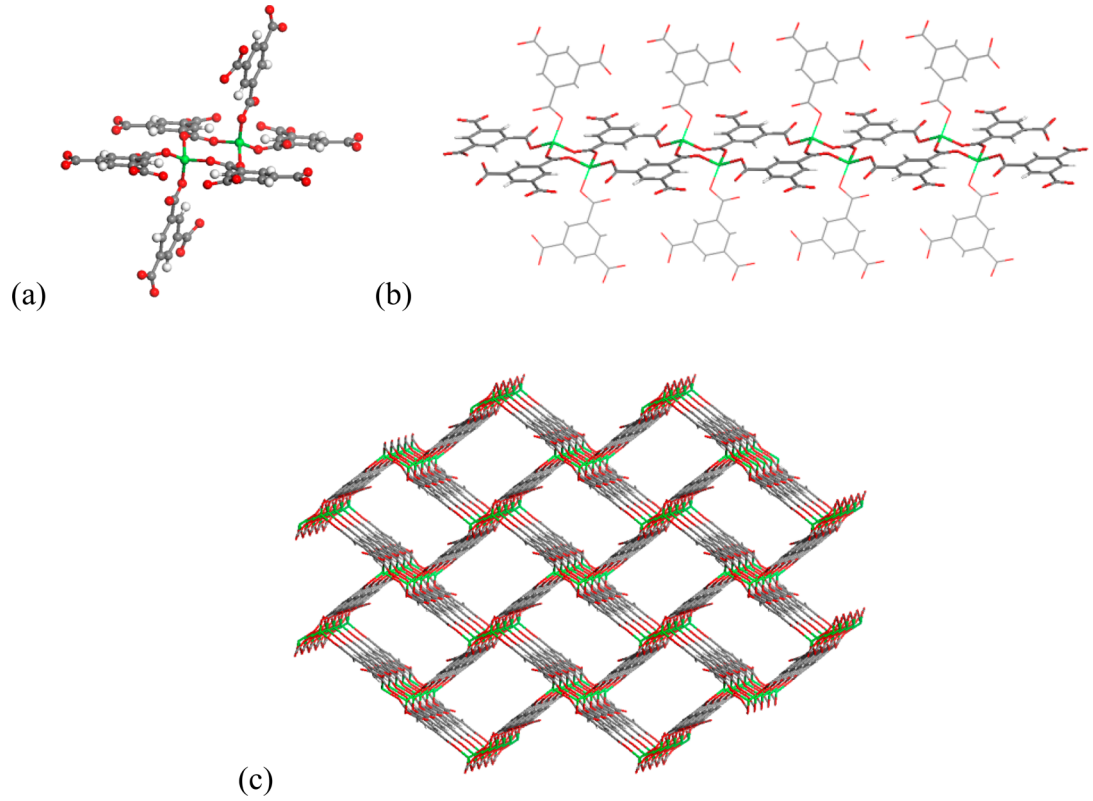

Figure 3. Crystal structure of {Zn-BTC}{$Me_2NH_2^+$}. (a) Coordination environment of Zn(II) cation and the $[Zn_2(\mu\text{-OOC})]_2$ structural motif. (b) A segment of one chain, with the chain shown in bold and axial ligation by BTC ligands from another carboxylate chains shown in feint. (c) The 3D grid viewed along the *a* axis with hydrogen atoms and guests atoms omitted for clarity.

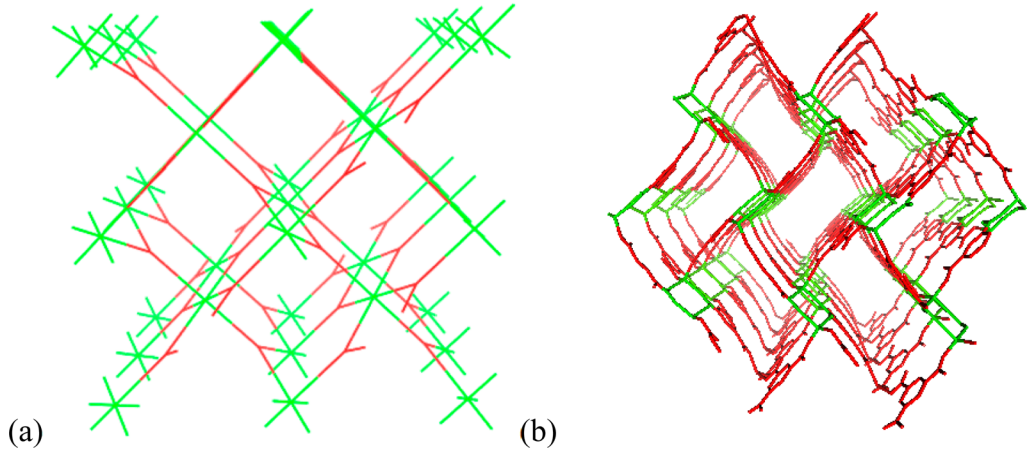

Figure 4. (a) (3,6)-Connected rutile TiO_2. Ti = green and O = red. (b) Crystal structure of framework {Zn-BTC}{$Me_2NH_2^+$} with Zn_2 SBUs in green and BTC ligands in red viewed along the *a* axis.

Cations of $Et_2NH_2^+$, *n*-$Bu_2NH_2^+$, Et_3NH^+, $(PhCH_2)Me_3N^+$, and BMIM all gave the same anionic Zn-BTC framework as in MOF {Zn-BTC}{$Me_2NH_2^+$}. However, differences in the size and shape, as well as in the interactions of cations with frameworks result in a different cation packing in the channels, and correspondingly different channels size within the frameworks, as shown in Figure 5 and Table 5.

Except the electrostatic interactions, additional hydrogen bonding interactions exist between the cations and the anionic Zn-BTC frameworks in MOFs with cations of $Me_2NH_2^+$, $Et_2NH_2^+$, *n*-$Bu_2NH_2^+$, and Et_3NH^+. The small size of $Me_2NH_2^+$ cations allows DMF solvents to coexist in the channels (Figure 5a). The relatively larger size of $Et_2NH_2^+$, *n*-$Bu_2NH_2^+$, and Et_3NH^+ excludes the extra solvent molecules and permits them to be incorporated into the channels by approaching the linear alkyl groups through the wall of the channels. The linear shape of $(PhCH_2)Me_3N^+$ and BMIM cations facilitates their accommodation in the centers of the channels, and in both cases only electrostatic interactions exist between the cations and Zn-BTC anionic frameworks. It was noted that in the case of $(PhCH_2)Me_3N^+$, the closest distance between the centroids of the nearby situated benzene rings of the cations was about 4.5 Å, which did not support ideal $\pi-\pi$ interactions between them.

dx.doi.org/10.1021/cg5006133 | *Cryst. Growth Des.* 2014, 14, 5452−5465

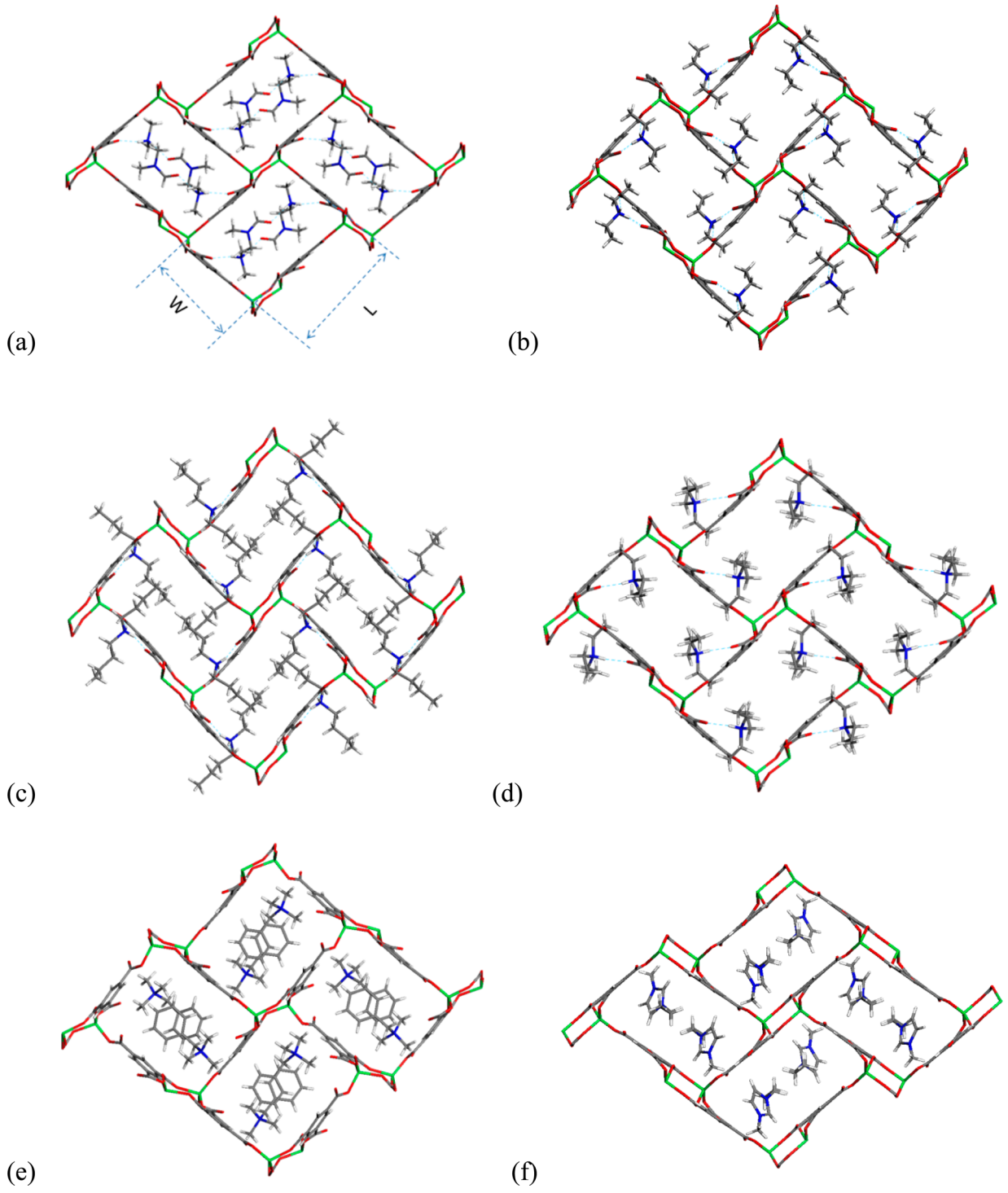

Figure 5. Cations packing position in the isoreticular Zn-BTC anionic frameworks viewed along the channels direction (a) $Me_2NH_2^+$, (b) $Et_2NH_2^+$, (c) n-$Bu_2NH_2^+$, (d) Et_3NH^+, (e) $(PhCH_2)Me_3N^+$, and (f) BMIM. Light blue dash lines represent H-bonding.

The geometry and the template cations' interaction preferences led to the variance of the channel structures in those isoreticular MOFs (as seen in Figure 5 and Table 5). For example, the length of the cross-section of the channels can extend from 10.97 to 12.40 Å in order to adapt cations from smaller $Me_2NH_2^+$ to larger n-$Bu_2NH_2^+$, and the width also changes from cation to cation. The separation between the nearby cations along the channel direction in those MOFs does not change very much. Only ∼3% relative changes were observed compared with the ∼13% changes of the length of the cross-section size.

However, when nonlinear quaternary ammonium cations such as n-Bu_4N^+ and Me_4N^+ were used, two new 3D anionic Zn-BTC frameworks were obtained. The size of the cations clearly affects the Zn-BTC coordinations in the new frameworks. The bulky n-Bu_4N^+ cations force the Zn-BTC frameworks to incorporate them inside the channels on one same layers and leave the other channels on the alternative layers open for solvents, as shown in Figure 6. In this new

dx.doi.org/10.1021/cg5006133 | Cryst. Growth Des. 2014, 14, 5452−5465

Table 5. Structural Parameters of the Channels in the Isoreticular {Zn-BTC}{cation} MOFs

cation	cross-section size of the channels (L × W) (Å)		Zn−Zn distance in the $[Zn_2(\mu\text{-}OOC)_2]$ (Å)	N···O distance in the N−H···O H-bonding (Å)	distance of N−N of the nearby organic cations along the channels (Å)
	L	*W*			
$Me_2NH_2^+$	10.97	**7.31**	3.8529(4)	2.722(2)	9.43
$Et_2NH_2^+$	11.37	**7.28**	3.8816(8)	2.722(3) and 2.748(3)	9.51
n-$Bu_2NH_2^{+a}$	12.40	**6.80**	3.975(2)	2.753(6) and 2.683(6)	9.49
Et_3NH^+	11.61	**7.59**	3.972(5)	2.724(6)	9.46
$(PhCH_2)Me_3N^+$	11.55	**8.55**	4.037(1)	/	9.57
BMIM	11.60	**6.95**	4.1142(9)	/	9.30

[a]This MOF is synthesized by method 1.

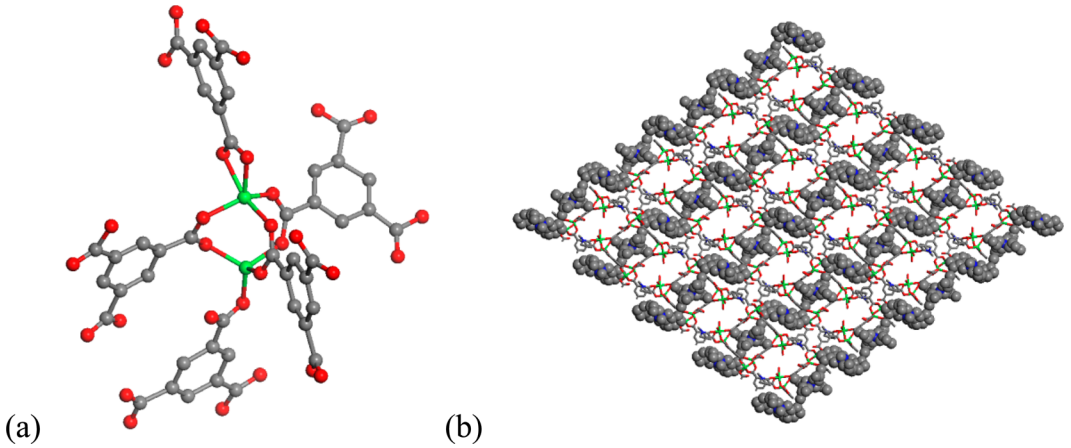

Figure 6. Crystal structure of {Zn-BTC}{*n*-Bu_4N^+}. (a) $[Zn_2(\mu\text{-}OOC)_3]$ dimer with coordinated five BTC ligands. (b) Cation locations in the Zn-BTC anionic framework viewed along the *b* axis.

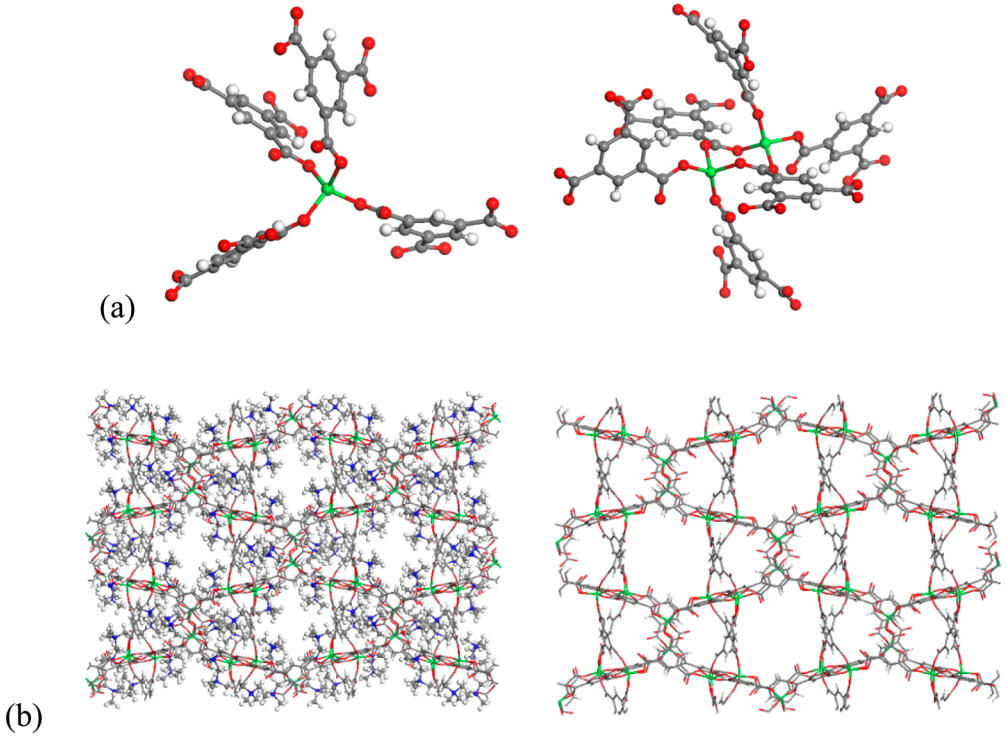

Figure 7. Crystal structure of {Zn-BTC}{Me_4N^+}. (a) The coordination environments of single tetrahedral Zn(II) ions and the $[Zn(\mu\text{-}OOC)]_2$ dimer. (b) Zn-BTC anionic frameworks with and without Me_4N^+ cations viewed along the *a* axis, NMP solvent molecules are omitted for clarity.

dx.doi.org/10.1021/cg5006133 | *Cryst. Growth Des.* 2014, 14, 5452−5465

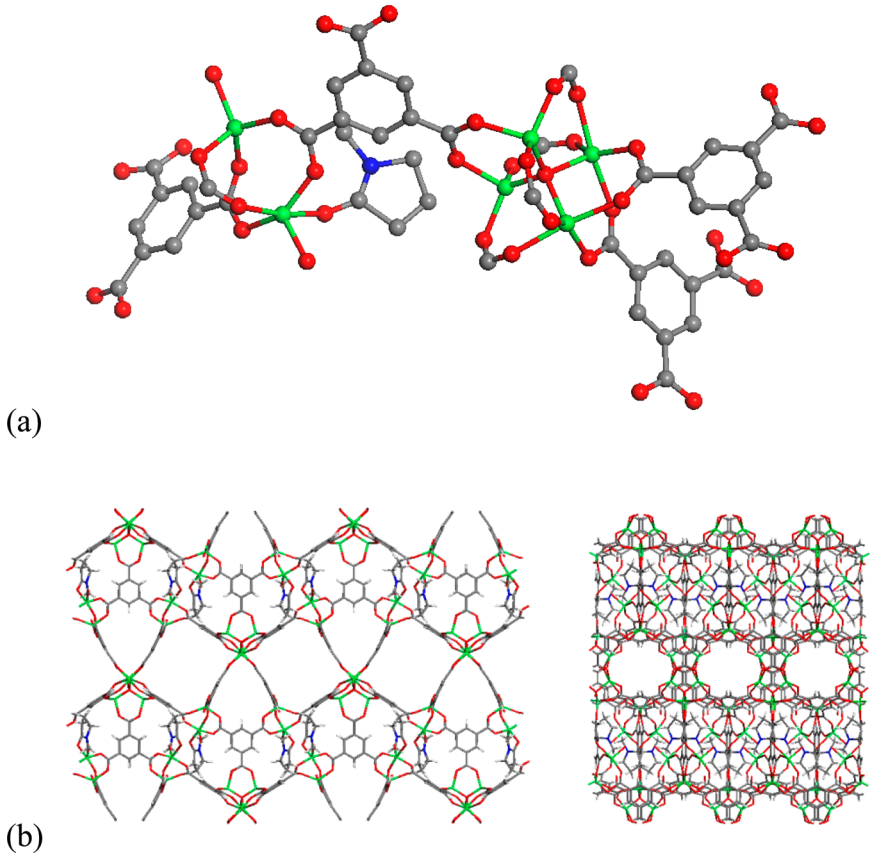

Figure 8. MOF {Zn-BTC}{n-$Bu_2NH_2^+$}-M2: (a) The Zn_2 dimer and Zn_4 cluster coordination environment. (b) The packing diagrams of the Zn-BTC anionic framework viewed along the a and c axes, respectively. Disordered NMP solvents are omitted for clarity.

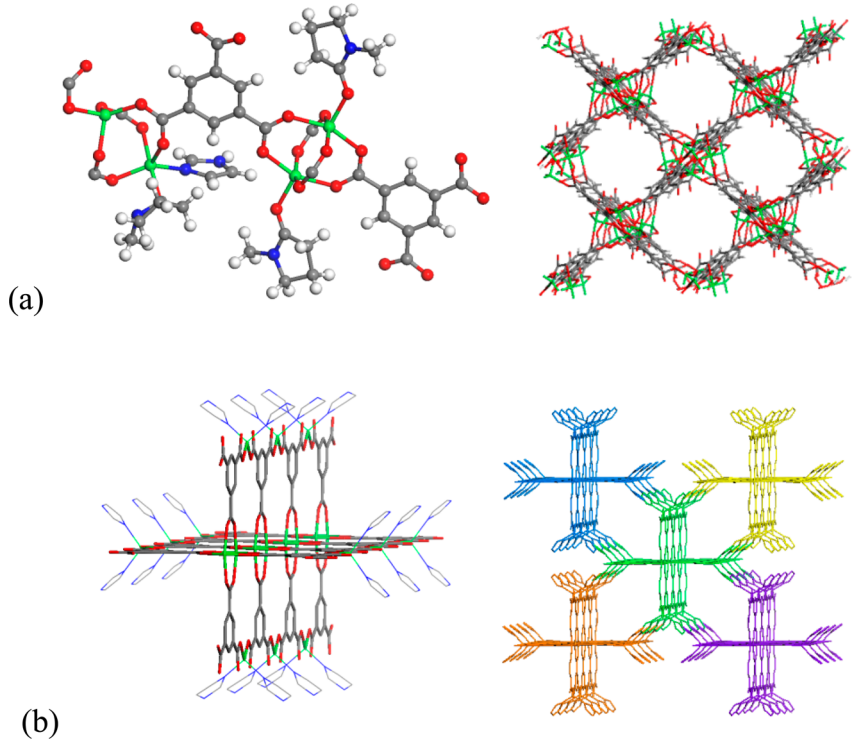

Figure 9. (a) MOF {Zn-BTC-IM}: the conjunction of two different dimeric units, and the 3D Zn-BTC framework structure viewed along the c axis. IM and NMP are omitted for clarity. (b) MOF {Zn-BTC-2IM}: the fragment of 1D polymeric chain and the hydrogen bonding association between chains viewed along the c-axis. Individual chains are shown in different colors for clarity.

dx.doi.org/10.1021/cg5006133 | *Cryst. Growth Des.* 2014, 14, 5452−5465

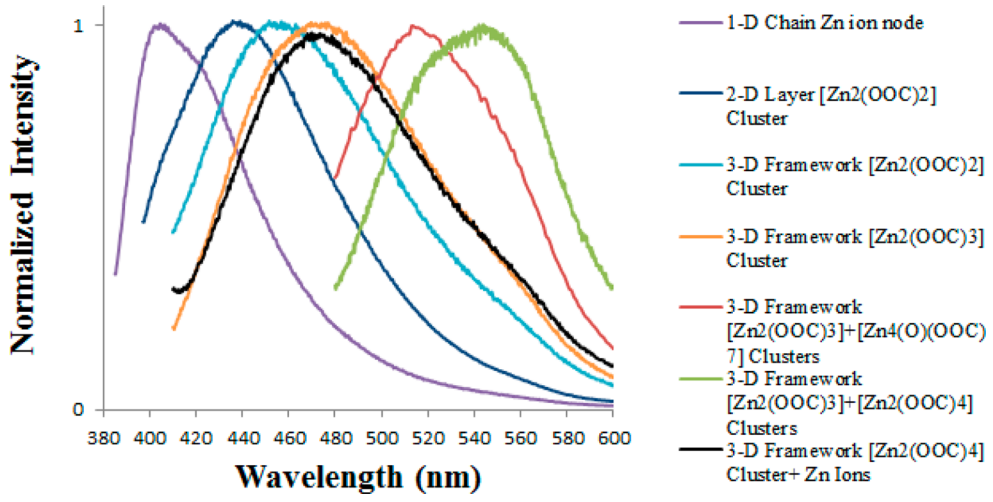

Figure 10. Fluorescent emission changes from different dimensional Zn-BTC structures.

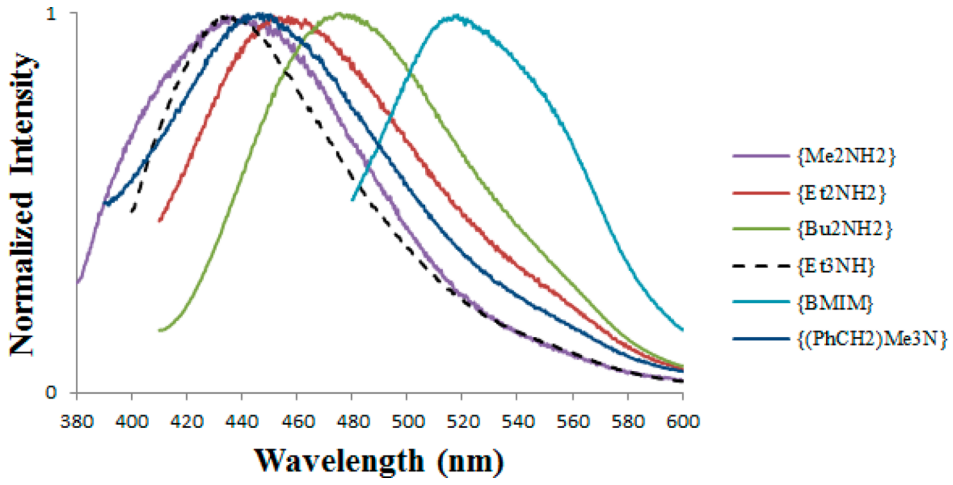

Figure 11. Fluorescent emission changes in the isoreticular Zn-BTC structures with different cations.

MOF, {Zn-BTC}{*n*-Bu_4N^+}, the Zn_2 dimer is in the [$Zn_2(\mu$-$OOC)_3$] configuration being surrounded by five BTC ligands. The BTC ligand uses the two-carboxylate groups to form the Zn_2 dimers in bridging binding mode and uses the other carboxylate in monodentate or chelate binding mode to connect the dimers into a channeled framework.

Me_4N^+ cations, even smaller in size compared to $(PhCH_2)$-Me_3N^+, generated a Zn-BTC anionic framework that differed from the previously discussed MOF {Zn-BTC}{$Me_2NH_2^+$}, as shown in Figure 7.

In MOF {Zn-BTC}{Me_4N^+}, two different coordination connectors of the Zn(II) exist. One is the isolated single Zn(II) which is tetrahedrally coordinated by four BTC ligands, and another is the [$Zn_2(\mu$-$OOC)_2$] dimer as seen in the MOF {Zn-BTC}{$Me_2NH_2^+$}. The anionic Zn-BTC frameworks are surrounded by the Me_4N^+ cations, and NMP solvent molecules occupy the remaining void space in the framework.

In this study, it was also observed that different methods for introducing the same cation could lead to different final framework structures. For example, when *N*,*N*-dibutylamine was used to form *n*-$Bu_2NH_2^+$ cations (method 2) instead of their in situ generation from decomposition of *N*,*N*-dibutylformamide (method 1), a new crystalline sample, MOF {Zn-BTC}{*n*-$Bu_2NH_2^+$}-M2, was obtained. In contrast to the MOFs generated from method 1, the new MOF {Zn-BTC}{*n*-$Bu_2NH_2^+$}-M2 contains two different Zn-BTC coordination motifs. One is the [$Zn_2(\mu$-$OOC)_3$] dimer, and another is the [$Zn_4(O)(\mu$-$OOC)_7$] cluster.[11] The Zn-BTC framework shows an alternative cage and channel structures connected between those Zn_2 and Zn_4 clusters by BTC ligands, as shown in Figure 8.

When imidazole (IM) was used as a base to generate imidazolium cations in the same Zn-BTC reaction system, the reaction failed. The introduced IM acted as an additional coordination ligand to Zn(II) ions resulting only in neutral frameworks. Two reaction composites of Zn(II):BTC:IM with a molar ratio of 1:1:1 and 1:1:2 resulted in two different Zn-BTC neutral MOFs, {Zn-BTC-IM} and {Zn-BTC-2IM}, respectively. MOF {Zn-BTC-IM} represents a 3D grid-like framework. It has two types of Zn(II)-BTC connection environments: one is the [$Zn_2(\mu$-$OOC)_3$] dimer, and another is the paddle-wheel [$Zn_2(\mu$-$OOC)_4$] dimer (Figure 9a). The Zn(II) ions of the dimers are also coordinated by NMP solvent molecules or IM ligands. However, MOF {Zn-BTC-2IM} shows an entirely different structure, where only [$Zn_2(\mu$-$OOC)_4$] dimers exist, and those dimers are connected with single Zn(II) ions through the BTC ligands to form a 1D chain (Figure 9b). Those single Zn(II) ions are coordinated by two

dx.doi.org/10.1021/cg5006133 | *Cryst. Growth Des.* 2014, 14, 5452−5465

Table 6. A Summary of the Cations H-Bond Forming Ability, the Corresponding Zn-BTC Structure, the Zn Coordination Motif, and the Fluorescent Emission Wavelength at Maximum Intensity

MOF	cation	number of H-bonding sites	dimensionality of Zn-BTC framework	number of (μ-OOC) involved in Zn cluster motif	FL emission @ maximum intensity (nm)
{Zn-BTC}{NH_4^+}	NH_4^+	4	1D	Zn(II), n = 0	405
{Zn-BTC}{$MeNH_3^+$}	$MeNH_3^+$	3	2D	$[Zn_2(\mu\text{-}OOC)_2]$, n = 2	440[a]
{Zn-BTC}{$Me_2NH_2^+$}	$Me_2NH_2^+$	2	3D	$[Zn_2(\mu\text{-}OOC)_2]$	434
{Zn-BTC}{$Et_2NH_2^+$}	$Et_2NH_2^+$	2	3D	$[Zn_2(\mu\text{-}OOC)_2]$	455
{Zn-BTC}{n-$Bu_2NH_2^+$ }-M1[b]	n-$Bu_2NH_2^+$ from formamide	2	3D	$[Zn_2(\mu\text{-}OOC)_2]$	476
{Zn-BTC}{Et_3NH^+}	Et_3NH^+	1	3D	$[Zn_2(\mu\text{-}OOC)_2]$	438
{Zn-BTC}{$(PhCH_2)Me_3N^+$}	$(PhCH_2)Me_3N^+$	0	3D	$[Zn_2(\mu\text{-}OOC)_2]$	445
{Zn-BTC}{BMIM }	BMIM	0	3D	$[Zn_2(\mu\text{-}OOC)_2]$	520
{Zn-BTC}{Me_4N^+}	Me_4N^+	0	3D	$[Zn_2(\mu\text{-}OOC)_2]$ + Zn(II)	450
{Zn-BTC}{n-Bu_4N^+}	n-Bu_4N^+	0	3D	$[Zn_2(\mu\text{-}OOC)_3]$, n = 3	470
{Zn-BTC}{n-$Bu_2NH_2^+$}-M2[b]	n-$Bu_2NH_2^+$ from amine	2	3D	$[Zn_2(\mu\text{-}OOC)_2]$ + $[Zn_4(O)(\mu\text{-}OOC)_7]$, n = 7	515
{Zn-BTC-IM}	IM as coordination ligand		3D	$[Zn_2(\mu\text{-}OOC)_3]$ + $[Zn_2(\mu\text{-}OOC)_4]$, n = 4	543
{Zn-BTC-2IM}	IM as coordination ligand		1D	$[Zn_2(\mu\text{-}OOC)_4]$ + Zn(II)	470

[a]The highest emission is at 370 nm when it is excited at 340 nm. [b]M1 and M2 indicate the cation's introduction method 1 and method 2, respectively.

extra IM ligands and form a tetrahedral N_2O_2 set. Each chain therefore has eight IM branches approaching out, and the chains are interconnected through the hydrogen bindings between those IM ligands to form a 3D network.

Effect of Cations to Fluorescence Changes. All of the formed Zn-BTC frameworks in this study show fluorescence emission in the visible spectrum at the solid state. The fluorescent spectra of maximum emission of each MOFs are shown in Figures 10 and 11.

A summary of the cations H-bond forming ability, the corresponding Zn-BTC structure, the Zn(II) coordination motif, and the fluorescent emission wavelength at maximum intensity are listed in Table 6.

As organized in Tables 5 and 6 and Figures 10 and 11, two interesting conclusions can be drawn for the anionic Zn-BTC structures:

(1) When the Zn-BTC anionic structure is changed from 1D chain to 2D layer, and finally to 3D framework, the emission wavelength shifts from violet (e.g., 405 nm) to blue (e.g., 455 nm) and even to the green light (e.g., 515 nm) region. Those changes are considered to be related clearly with dimensionality of the crystal structures. More specifically, it is noticed those changes have a close relationship with what type of Zn-nodes the framework contains. In this study, the Zn-nodes existing in the frameworks include the isolated single Zn(II) ions and the (μ-OOC) bridged Zn(II)-clusters, such as $[Zn_2(\mu\text{-}OOC)_2]$, $[Zn_2(\mu\text{-}OOC)_3]$, $[Zn_2(\mu\text{-}OOC)_4]$, and $[Zn_4(O)(\mu\text{-}OOC)_7]$. The emission behavior for those Zn-BTC MOFs suggests that when more bridging binding mode carboxylates (μ-OOC) are used to build the Zn-nodes in frameworks, the longer wavelength emission of MOFs can be expected. For example, in the case of NH_4^+, only single Zn(II) ions act as connection nodes, and the BTC ligands coordinated to the Zn_2 nodes in a monodentate binding mode. The emission from this framework emits a violet light at 405 nm, which is close to the H_3BTC ligand itself (emission at ~365 nm). However, when the $MeNH_3^+$ is used, the framework has a 2D layer structure with $[Zn_2(\mu\text{-}OOC)_2]$ dimers as the connection nodes, and as we can see in Figure 10, the indigo emission at 440 nm is observed. Moreover, this framework releases an emission peak at 370 nm under an excitation wavelength of 340 nm, which can be assigned to the BTC ligand-centered charge transitions.[12] When the cations are changed to less than two hydrogen-bond forming cations, such as n-Bu_4N^+, where 3D frameworks are obtained and $[Zn_2(\mu\text{-}OOC)_3]$ acts as connection node, the emission shifts to the blue light region at 470 nm. However, when it is in the Me_4N^+ case, the framework uses both $[Zn_2(\mu\text{-}OOC)_2]$ and single Zn(II) as connection nodes in the structure. Because fewer (μ-OOC) used in those Zn-nodes, the emission wavelength shifts toward the violet direction and gives an emission at 450 nm, compared to the n-Bu_4N^+ case. When the 3D frameworks contain both $[Zn_2(\mu\text{-}OOC)_2]$ and $[Zn_4(O)(\mu\text{-}OOC)_7]$ clusters as nodes, as in the case of MOF {Zn-BTC}{n-$Bu_2NH_2^+$ }-M2, the emission wavelength shifts to 515 nm, producing a green light.

(2) Frameworks, which have the same Zn-BTC anionic structure as shown in Figure 5, provided us good examples for understanding how the differences in the inclusive cations influence the fluorescence of the frameworks. It is suggested that the fewer the interactions between the cations and anionic frameworks in the MOFs, the longer wavelength of emission the MOFs can have. For example, as listed in Table 5, for cations that can form additional hydrogen bonding with the frameworks, i.e., $Me_2NH_2^+$, Et_3NH^+, $Et_2NH_2^+$, and n-$Bu_2NH_2^+$, the pK_a of the corresponding amines increases (pK_a for Me_2NH = 10.64, Et_3N = 10.65, Et_2NH =10.98, and $(n\text{-}Bu)_2NH$ = 11.25),[13] which suggests the strength of hydrogen bonding N–H···O can decrease in the same order. For the similar ammonium cations $R_2NH_2^+$, from Me- to Et-, and further to Bu-substituted ones, one might conclude that the interaction between cations and framework becomes weaker and weaker in the same order, and as it was observed, the emission changed

dx.doi.org/10.1021/cg5006133 | Cryst. Growth Des. 2014, 14, 5452–5465

from indigo light at 434 nm to 455 nm and finally to blue light at 476 nm, respectively. When we compare the BMIM and $(PhCH_2)Me_3N^+$ cations which cannot have hydrogen bonding with the frameworks, the imidazolium cation gave a green emission at 520 nm, while $(PhCH_2)Me_3N^+$ gave an indigo emission at 445 nm. This could also result from the BMIM having a distributed positive charge along the imidazole ring, compared to the relatively localized charge in the $(PhCH_2)$-Me_3N^+ cation, which as a result, influences the electrostatic interactions within the framework. Cations $(PhCH_2)Me_3N^+$ can only have electrostatic interactions with the frameworks when compared with the secondary dialkylammonium cations that can have additional hydrogen bonding with the frameworks. However, the $(PhCH_2)Me_3N^+$ cation gave a similar emission at 445 nm as the $Me_2NH_2^+$ and $Et_2NH_2^+$ cations, which shifted to the violet region direction unlike the $(n\text{-}Bu)_2NH_2^+$ cations. The reason why remains unclear. The changes of the emission wavelength in those MOFs seem to have a similar pattern with the width of the cross-section size of the channels (as listed in bold in Table 5). Future computational research may give some clues about how the structural changes of the channels influence the fluorescence. One thing evident from this study is that cations acted as electron withdrawing agents from the anionic Zn-BTC frameworks. The stronger the interactions, the fewer the number of electrons that may be distributed along the conjugated Zn-BTC framework and the greater the shift in the resulting emission to the shorter wavelength direction.

Although the above two observations were concluded from the anionic frameworks, they can be applied to the two IM coordinated neutral frameworks. As seen in Figure 9, MOF {Zn-BTC-IM} has a 3D framework and contains both $[Zn_2(\mu\text{-}OOC)_3]$ and $[Zn_2(\mu\text{-}OOC)_4]$ clusters as connection nodes, while MOF {Zn-BTC-2IM} has 1D chain structures that are cross-linked through hydrogen bonding to form a framework and contains the cluster $[Zn_2(\mu\text{-}OOC)_4]$ and single Zn(II) ions as the connection nodes. As deduced from conclusion 1, MOF {Zn-BTC-IM} should give a longer wavelength emission than MOF {Zn-BTC-2IM}. As observed in this study, MOF {Zn-BTC-IM} gave a yellow emission at 543 nm, and MOF {Zn-BTC-2IM} gave a blue emission at 470 nm. The overall longer emission wavelength of both Zn-BTC-IM frameworks compared to the anionic Zn-BTC frameworks may arise from the electron contribution of the coordinated IM ligands, which is also consistent with conclusion 2.

CONCLUSION

In summary, a series of anionic Zn-BTC frameworks with NH_4^+ or organic cations residing in the voids of the frameworks were analyzed via single-crystal X-ray crystallography, and the corresponding fluorescence of the frameworks was studied. It was observed that cations acting as structure-directing agents affect the coordination structure of the Zn-BTC anionic frameworks. Most of the frameworks contain (μ-OOC) bridged Zn(II)-clusters as connecting nodes, such as $[Zn_2(\mu\text{-}OOC)_2]$, $[Zn_2(\mu\text{-}OOC)_3]$, $[Zn_2(\mu\text{-}OOC)_4]$, and $[Zn_4(O)(\mu\text{-}OOC)_7]$.

All of the Zn-BTC anionic frameworks reported herein showed fluorescent emission in the visible spectrum region. The fluorescent emissions are closely related to the (μ-OOC) bridged Zn(II)-clusters. The more the Zn(II) and (μ-OOC) bridging BTC contributed to the cluster, the longer the observed emission wavelength. In the same isoreticular Zn-BTC anionic frameworks, the strength of interactions between the inclusive cations and framework influences the emission as well. Lesser interactions result in emission shifts to the longer wavelength direction.

ASSOCIATED CONTENT

Supporting Information

PXRD patterns as well as X-ray crystallographic files (CIF) are available for all compounds. These materials are available free of charge via the Internet at http://pubs.acs.org.

AUTHOR INFORMATION

Corresponding Authors

*(Q.W.) Current address: Department of Biology and Chemistry, New Mexico Highlands University, NM 87701, USA. E-mail: qwei@nmhu.edu.

*(T.T.) Current address: Department of Biology and Chemistry, New Mexico Highlands University, NM 87701, USA. E-mail: tvtimofeeva@nmhu.edu.

Notes

The authors declare the following competing financial interest(s): The MOFs reported in this manuscript have been filed in a provisional application for patent.

ACKNOWLEDGMENTS

Authors are grateful for support from NSF DMR-0934212, PREM, and EPSCoR IIA-1301346.

REFERENCES

(1) (a) Kenarsari, S. D.; Yang, D.; Jiang, G.; Zhang, S.; Wang, J.; Russell, A. G.; Wei, Q.; Fan, M. *RSC Adv.* **2013**, 22739. (b) Wei, Q.; Yang, D.; Fan, M.; Harris, H. G. *Crit. Rev. Environ. Sci. Technol.* **2013**, 2389.

(2) (a) Farha, O. K.; Hupp, J. T. *Acc. Chem. Res.* **2010**, *43* (8), 1166. (b) Czaja, A. U.; Trukhan, N.; Müller, U. *Chem. Soc. Rev.* **2009**, *38* (5), 1284. (c) James, S. L. *Chem. Soc. Rev.* **2003**, *32* (5), 276. (d) Wu, H.; Gong, Q.; Olson, D. H.; Li, J. *Chem. Rev.* **2012**, *112* (2), 836. (e) Ma, L.; Abney, C.; Lin, W. *Chem. Soc. Rev.* **2009**, *38* (5), 1248. (f) Chen, S.; Zhang, J.; Wu, T.; Feng, P.; Bu, X. *J. Am. Chem. Soc.* **2009**, *131* (44), 16027. (g) Long, J. R.; Yaghi, O. M. *Chem. Soc. Rev.* **2009**, *38* (5), 1213. (h) Reich, T. E.; Jackson, K. T.; Li, S.; Jena, P.; El-Kaderi, H. M. *J. Mater. Chem.* **2011**, *21* (29), 10629.

(3) (a) O'Keeffe, M.; Yaghi, O. M. *Chem. Rev.* **2011**, 675. (b) Kim, J.; Chen, B.; Reineke, T. M.; Li, H.; Eddaoudi, M.; Moler, D. B.; O'Keeffe, M.; Yaghi, O. M. *J. Am. Chem. Soc.* **2001**, *123*, 8239.

(4) (a) Furukawa, H.; Cordova, K. E.; O'Keeffe, M.; Yaghi, O. M. *Science* **2013**, *341* (6149), 1230444. (b) Kuppler, R. J.; Timmons, D. J.; Fang, Q. R.; Li, J. R.; Makal, T. A.; Young, M. D.; Yuan, D.; Zhao, D.; Zhuang, W.; Zhou, H. C. *Coord. Chem. Rev.* **2009**, *253* (23), 3042. (c) Li, J. R.; Kuppler, R. J.; Zhou, H. C. *Chem. Soc. Rev.* **2009**, *38* (5), 1477. (d) Chen, B.; Xiang, S.; Qian, G. *Acc. Chem. Res.* **2010**, *43* (8), 1115.

(5) (a) Bauer, C. A.; Timofeeva, T. V.; Setterson, T. B.; Patterson, B. D.; Liu, V. H.; Simmons, B. A.; Allendorf, M. D. *J. Am. Chem. Soc.* **2007**, *129*, 7136. (b) Allendorf, M. D.; Bauer, C. A.; Bhakta, R. K.; Houk, R. J. T. *Chem. Rev.* **2009**, *38* (5), 1330. (c) Basabe-Desmonts, L.; Reinhoudt, D.; Crego-Calama, M. *Chem. Soc. Rev.* **2007**, *36*, 993. (d) Cui, Y.; Yue, Y.; Qian, G.; Chen, B. *Chem. Rev.* **2011**, *112* (2), 1126.

(6) (a) Wei, Q.; Nieuwenhuyzen, M.; Meunier, F.; Hardacrea, C.; James, S. L. *J. Chem. Soc., Dalton Trans.* **2004**, 1807. (b) Wei, Q.; James, S. L. *Chem. Commun.* **2005**, 1555. (c) Wei, Q.; Yang, D.; Larson, T. E.; Kinnibrugh, T. L.; Zou, R.; Henson, N. J.; Timofeeva, T. V.; Xu, H.; Zhao, Y.; Mattes, B. R. *J. Mater. Chem.* **2012**, 10166. (d) Zou, R.; Abdel-Fattah, A. I.; Xu, H.; Burrell, A. K.; Larson, T. E.; McCleskey, T. M.; Wei, Q.; Janicke, M. T.; Hickmott, D. D.; Timofeeva, T. V.; Zhao, Y. *Cryst. Growth Des.* **2010**, *10*, 1301.

(e) Croitor, L.; Coropceanu, E. B.; Siminel, A. V.; Kravtsov, V. C.; Fonari, M. S. *Cryst. Growth Des.* **2011**, *11* (8), 3536. (f) Croitor, L.; Coropceanu, E. B.; Jeanneau, E.; Dementiev, I. V.; Goglidze, T. I.; Chumakov, Y. M.; Fonari, M. S. *Cryst. Growth Des.* **2009**, *9* (12), 5233.
(7) (a) Della Rocca, J.; Liu, D.; Lin, W. *Acc. Chem. Res.* **2011**, *44*, 957. (b) Lu, W. G.; Jiang, L.; Feng, X. L.; Lu, T. B. *Inorg. Chem.* **2009**, *48*, 6997. (c) Chen, D. S.; Sun, L. B.; Liang, Z. Q.; Wang, C. G.; Su, Z. M.; Xing, H. Z. *Cryst. Growth Des.* **2013**, *13*, 4092. (d) Song, W. C.; Li, J. R.; Song, P. C.; Tao, Y.; Yu, Q.; Tong, X. L.; Bu, X. H. *Inorg. Chem.* **2009**, *48*, 3792. (e) Lu, W. G.; Jiang, L.; Feng, X. L.; Lu, T. B. *Inorg. Chem.* **2009**, *48* (15), 6997.
(8) *SAINTP+ for NT. Data Reduction and Correction Program*, v. 6.2; Bruker AXS: Madison, Wisconsin, USA2001.
(9) Sheldrick, G. M. *SHELXTL NT*, v. 6.12, Structure Determination Software Suite; Bruker AXS: Madison, Wisconsin, USA, 2001.
(10) (a) Yang, S.; Lin, X.; Blake, A. J.; Walker, G. S.; Hubberstey, P.; Champness, N. R.; Schröder, M. *Nat. Chem.* **2009**, *1* (6), 487. (b) Xie, L.; Liu, S.; Gao, B.; Zhang, C.; Sun, C.; Li, D.; Su, Z. *Chem. Commun.* **2005**, *18*, 2402.
(11) Gao, J.; Ye, K.; Yang, L.; Xiong, W. W.; Ye, L.; Wang, Y.; Zhang, Q. *Inorg. Chem.* **2014**, *53* (2), 691.
(12) Fang, Q.; Zhu, G.; Xue, M.; Sun, J.; Sun, F.; Qiu, S. *Inorg. Chem.* **2006**, *45*, 3582.
(13) Hall, H. K., Jr. *J. Am. Chem. Soc.* **1957**, *79*, 5441.